Available online at www.sciencedirect.com

SciVerse ScienceDirect

journal homepage: www.elsevier.com/locate/he

Fabrication of electrolyte supported micro-tubular SOFCs using extrusion and dip-coating

Wen-Shuo Hsieh [a], Pang Lin [a], Sea-Fue Wang [b,*]

[a] Department of Materials Science and Engineering, National Chiao Tung University, Hsinchu City 300, Taiwan, ROC
[b] Department of Materials and Mineral Resources Engineering, National Taipei University of Technology, 1, Sec. 3, Chung-Hsiao E. Rd., Taipei City 106, Taiwan, ROC

ARTICLE INFO

Article history:
Received 30 July 2012
Received in revised form
7 December 2012
Accepted 9 December 2012
Available online 11 January 2013

Keywords:
Solid oxide fuel cell
Tubular
Extrusion
Dip-coating
Sintering

ABSTRACT

Dense electrolyte supported micro tubular solid oxide fuel cells (T-SOFCs) were prepared in this study. Green $Zr_{0.8}Sc_{0.2}O_{2-\delta}$ (ScSZ) electrolyte micro-tubes with a thickness of 300 μm were successfully prepared by extrusion at room temperature. After firing at 1400 °C, the bare electrolyte micro-tube with a thickness of 210 μm, a diameter of 3.8 mm, and a length of 40 mm reached a relative density of 96.84% and a flexural strength of 202 MPa. To achieve a better sintering shrinkage match, the electrolyte micro-tubes were pre-sintered at 1100 °C, coated with NiO/ScSZ (60 vol.%:40 vol.%) in the inner surface of the micro-tubes by dip-coating method, and then co-fired at 1400 °C. After co-sintering, the interface of the porous anode layer and the dense electrolyte layer demonstrated good adhesion and mechanical integrity. Subsequently, a $La_{0.8}Sr_{0.2}MnO_{3-\delta}$ (LSM)/$Ce_{0.8}Gd_{0.2}O_{2-\delta}$ (GDC) (80 vol.%:20 vol.%) cathode layer was coated on the outer surface of the micro-tubes by dip-coating method and post-sintered at 1100 °C. The thicknesses of the anode and cathode layers read approximately 28 and 34 μm respectively. After thermal cycling between 30 °C and 800 °C under 97% N_2–3%H_2 on the anode and air on the cathode, the micro T-SOFCs showed no delamination and retained good adhesion based on the SEM results. The maximum power densities (MPD) of the single cell read 0.26 and 0.23 W cm^{-2} respectively at 920 and 900 °C, and the open circuit voltage (OCV) reported the same 1.08 V.

1. Introduction

The world to date has continued to rely on fossil fuels as its major energy source. In response to alarming issues like the world's ever-increasing energy consumption, energy security concerns, global warming, and acid rain, using renewable energy and developing more efficient energy conversion devices have emerged as significant R&D trends. Solid oxide fuel cells (SOFCs), known as high-efficiency energy conversion devices, change chemical energy into electrical energy through the reaction of oxygen (cathode side) and hydrocarbon fuel (anode side). SOFCs with various configurations, including planar, monolithic and tubular designs, have been developed. Compared to other configurations, tubular SOFCs reveal excellent thermal resistance, secure sealing, solid mechanical strength, rapid heat cycling, and stable performance at high temperatures (700 °C–1000 °C) [1–3]. The fabrication of tubular SOFCs usually consists of tube forming

* Corresponding author. Tel.: +886 2 2771 2171x2735; fax: +886 2 2731 7185.
E-mail address: sfwang@ntut.edu.tw (S.-F. Wang).
0360-3199/$ – see front matter
http://dx.doi.org/10.1016/j.ijhydene.2012.12.056

and layer deposition. Ceramic micro-tubes can be prepared using extrusion, gel casting, isostatic pressing, or phase inversion methods, while layer deposition further includes dip-coating, plating, and spray-coating [4–8].

Siemens Westinghouse multiple tubular SOFCs had been successfully tested for 70,000 h [9]. Kendall and Palin [10] and Herlea et al. [11] reported that their small tubular SOFCs were able to tolerate rapid heating and cooling at an operating temperature of 800 °C and marked with high power density. Suzuki et al. [4] presented single micro-tubular SOFCs 0.8 mm in diameter, 8 mm in length, and capable of generating a power density over 1.0 W cm^{-2} at 550 °C. These tubular SOFCs showed good mechanical properties and resistance to thermal stresses when subjected to cyclic rapid heating and cooling. Most of them were anode-supported micro-tubes exhibiting excellent performance. Nevertheless, anode-supported tubular SOFCs are still far from commercial availability, mainly due to their unstable operating life [12]. For instance, anode reduction at high temperature tends to create a porous cermet structure, which induces a volume exchange of the anode and may easily crack the thin electrolyte layer [5]. The electrolyte-supported design is generally agreed to possess superior stability as compared to its anode-supported counterpart. In addition, micro-tubular SOFCs with thin double layer electrolytes of zirconia and ceria have been reported to feature low impedance at operating temperatures of <800 °C [11]. For its strength in maintaining mechanical integrity, electrolyte-supported micro-tubular designs can be expected to remain viable for future SOFC applications. In this study, therefore, the effects of paste formulation and sintering process on the mechanical integrity of micro-tubular SOFCs, fabricated via extrusion and dip-coating techniques, were investigated. Exhibiting the highest oxide-ion conductivity among the zirconia systems and excellent mechanical strength in oxidizing and reducing atmospheres, scandium-stabilized zirconia (ScSZ) was used as the electrolyte material [2]. The optimum firing conditions for preventing the formation of physical defects in the tubular cells were developed.

2. Experimental

2.1. Fabrications of the green electrolyte micro-tubes

In this study, electrolyte pastes were prepared from $Zr_{0.8}Sc_{0.2}O_{2-\delta}$ (ScSZ; $d_{50} = 0.09$ μm; Fuel Cell Materials), binder (Methyl cellulose, MC, Tsair Yu Technology), lubricant (Oil, Tsair Yu Technology), surfactant and D.I. water. The mixtures were then aged in a plastic container for ≈6 h. Workable pastes were extruded into the micro-tubes by a custom-design extrusion machine. The speed of extrusion piston was set at 1.5 mm/s. After drying, the green micro-tubes with a diameter of 5 mm and a wall thickness of approximately 300 μm were cut to 50 mm in length. The electrolyte micro-tubes were then sintered at 1100 °C, 1350 °C, 1400 °C and 1450 °C. Scanning electron microscopy (SEM, Hitachi S4700) was used to examine the microstructures on the surfaces and fracture surfaces of the micro-tubes. To calculate the average grain size, the fracture surfaces of the electrolyte were polished and then thermally etched at one hundred degrees below the initial sintering temperature. The density of the electrolyte micro-tubes was characterized using the water immersion (Archimedes) method and the porosity estimated. The flexural strength of the ScSZ micro-tubes sintered at different temperatures was determined by third-point loading (SHIMADZU; AG-IC) and expressed as Modulus of Rupture (MR) in psi (MPa). The force at the breaking point was recorded and used to calculate the bending strength (σ_F) according to the following equation [13].

$$\sigma_F = \frac{8FLD}{\pi(D^4 - d^4)} \quad (1)$$

where F is the measured load at fracture and L, D, and d are respectively the length (30 mm) and the outer and inner diameters of the micro-tubes.

2.2. Co-sintering of the bi-layers

In order to evaluate the co-sintering characteristics of the electrolyte–anode bi-layers, dilatometric analysis was performed to examine the sintering shrinkage of the ceramics with respect to temperature. The anode and electrolyte compacts were formed directly from the electrolyte paste used for extrusion and anode slurry used for dip coating. Dilatometric analysis was further performed on the green anode compact and the green electrolyte compact as well as on those pre-sintered at 1100, 1200 and 1400 °C for 2 h. Experiments were conducted using a dilatometer (NETZSCH DIL 402C) under air and at a heating rate of 5 °C/min. This method makes it possible to trace the onset temperature of the densification during sintering.

2.3. Coating of anode and cathode layers

To reduce the sintering shrinkage mismatch of the anode–electrolyte bi-layer, the electrolyte micro-tubes were pre-fired at 1100 °C, 1200 °C and 1450 °C before electrode coating. A thin anode layer coating on the inner surface of the micro-tubes was fabricated through dip-coating in a colloidal suspension. The composition of anode slurry is given in Table 1. NiO (Fuel Cell Materials, $d_{50} = 0.8$ μm) and ScSZ powders were mixed at a volume ratio of 6:4. In addition, 30 vol.% carbon powders were added to produce sufficient porosity and to reduce the sintering mismatch with the electrolyte. The mixed powders were first ball-milled with ethanol and toluene (ratio of 3:2) for 1 h at a mill speed of 350 rpm. A binder (Ferro; B74001) was then added to the anode slurry and ball-milled for 7 h. The anode slurry was then dip-coated onto the inner surfaces of the electrolyte micro-tubes. After drying, the half-cells were co-sintered at 1200 °C, 1300 °C and 1400 °C for 2 h in air.

The formulation of cathode slurry was listed in Table 2. $Ce_{0.8}Gd_{0.2}O_{2-\delta}$ (GDC; Fuel Cell Materials, $d_{50} = 0.09$ μm) powders and $La_{0.8}Sr_{0.2}MnO_{3-\delta}$ (LSM, Fuel Cell Materials, $d_{50} = 1.19$ μm) were mixed in a volume ratio of 8:2. The mixed powders were ball-milled with ethanol and toluene (ratio of 3:2). After ball-milling, the cathode slurry was poured into a container and dip-coated onto the outer surfaces of the

Table 1 – Formulations of electrolyte pastes and characteristics of extruded green micro-tubes.

Sample no.	Additives				MC:Oil	Characteristics of the green micro-tubes
	MC (wt%)	Oil (wt%)	D.I. Water (wt%)	Surfactant. (wt%)		
ScSZ-10a	1.0	4.5	28.0	0	1:4.5	Pinholes on surface, sticky paste, tube elongated
ScSZ-10b	1.0	3.0	28.0	0	1:3.0	Worm-shaped, not smooth to extrude
ScSZ-15a	1.5	3.0	28.0	0	1:2.0	Good shape, slightly rough surface
ScSZ-15b	1.5	3.0	27.4	0	1:2.0	Worm shape, not smooth to extrude
ScSZ-15c	1.5	4.5	28.0	0	1:3.0	Pinholes on surface, sticky paste, tube elongated
ScSZ-20a	2.0	4.0	28.0	0	1:2.0	Good shape, low green density
ScSZ-20b	2.0	2.0	28.0	0	1:1.0	Rough surface, not smooth to extrude
ScSZ-21a	2.1	2.8	22.0	0.6	1:1.3	Good shape, rough surface after drying
ScSZ-21b	2.1	2.0	22.0	0.6	1:1.0	Good shape, smooth surface

Table 2 – Formulations of anode and cathode slurries.

Slurry	Functional powders (wt%)	Carbon powder (wt%)	Binder (wt%)	Solvent (wt%)
Anode slurry	34.5	3.4	10.3	51.8
Cathode slurry	43.5	0	13.0	43.5

electrolyte micro-tubes. After drying, the micro-tubular SOFCs were post-sintered at 1100 °C for 2 h in air.

3. Results and discussion

3.1. *Preparation of electrolyte micro-tubes*

In order to operate at a low temperature, the tubular electrolyte was fabricated to possess a minimum thickness ranging from 200 to 210 μm after sintering. Mixing procedure, extrusion parameters, powder characteristics and organic additives all play important roles in the quality of the final extruded products (micro-tubes). Table 1 shows formulations of the electrolyte pastes and the characteristics of the corresponding green micro-tubes extruded. Under identical mixing procedure, extrusion parameters, and ScSZ powders, the effects of the organic additives on the characteristics of the extruded micro-tubes were investigated and presented in Table 1. It was evident that the properties of the green micro-tubes depended to a great extent on the additive content.

It was found that extrusion of ScSZ-15b paste containing 27.4 wt% water was not successful due to insufficient moisture. The optimum water content, which strongly depends on the particle size of the ScSZ powders, emerged to be 28.0 wt%. Results indicated that the addition of at least 1.5 wt% MC to the ScSZ powders was necessary to obtain an extrudable paste because of the small particle size ($d_{50} = 0.8$ μm) and the large surface area (9.21 m^2/g) of the ScSZ powders. For the ScSZ-10b, its 1.0 wt% MC was not enough to completely cover the surfaces of the particles, thus resulting in non-smooth extrusion. It was also observed that, in addition to the MC content, the oil/MC ratio was critical to the extrusion behavior. For formulations with an oil/MC ratio $\geq$3, such as SCSZ-10a and ScSZ-15c, the pastes were too sticky to ensure problem-free formation as the micro-tubes were marked with some pinholes on the surfaces and became narrowed and lengthened. On the other hand, the ScSZ-15a and ScSZ-20a pastes (oil/MC ratio $\approx$ 2) could be extruded into micro-tubes with an acceptable appearance while some drawbacks, notably a slightly rough surface and a low green density, were observed due to the high levels of additives (32.5 wt% and 34.0 wt% respectively). It is necessary to reduce the additive contents in the pastes in order to obtain dense electrolyte micro-tubes with a smooth surface. An effective approach is to use a surfactant for bridging the ceramic powders and the binder, thereby reducing the degree of agglomeration. The study had accordingly added 0.6 wt% surfactant to the ScSZ-21a and ScSZ-21b pastes and found the additive contents significantly reduced to respectively 27.5 wt% (oil/MC $\approx$ 1.3) and 26.7 wt% (oil/MC $\approx$ 1.0) without sacrificing the rheology of the pastes. Both the ScSZ-21a and ScSZ-21b pastes produced well-shaped micro-tubes; the former, however, generated a rough surface after drying. Also to be noted is that, though the ScSZ-20b and ScSZ-21b pastes had a similar oil/MC ratio ($\approx$1.0), the latter, containing 22 wt% water and an additional 0.6 wt% surfactant, showed an excellent rheological property for extrusion and produced dense electrolyte micro-tubes with a smooth surface while the former, containing 28 wt% water without any surfactant, gave birth to a rough surface on the extruded micro-tubes.

3.2. *Characteristics of the sintered electrolyte micro-tubes*

As indicated by Fig. 1 that shows the lateral shrinkage and relative density of the ScSZ micro-tubes at various sintering temperatures, the sintered density increased rapidly with the sintering temperature, approaching 92.1% theoretical density (T.D.) at 1350 °C, proceeding to reach the maximum density of

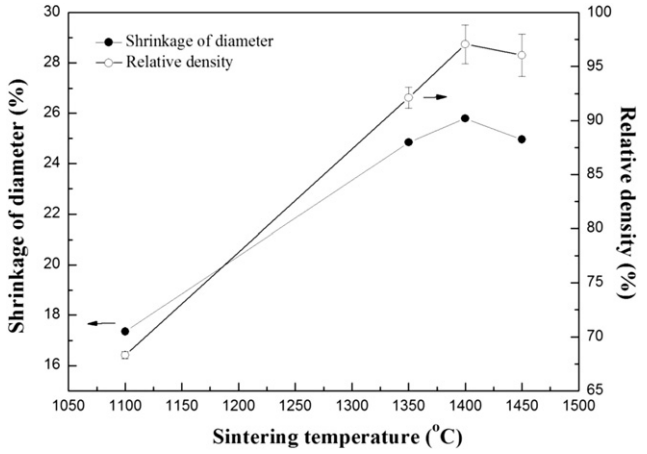

Fig. 1 – Sintering shrinkage and relative density of ScSZ micro-tubes sintered at different temperatures.

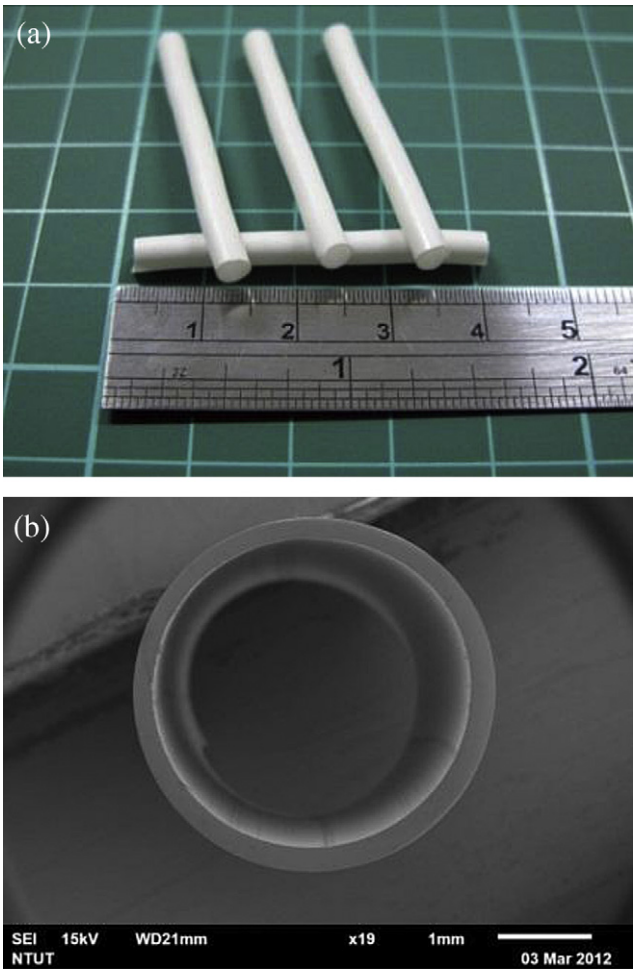

Fig. 2 – (a) Photograph and (b) SEM micrograph of ScSZ micro-tubes sintered at 1400 °C.

97.1% T.D. at 1400 °C, and then leveling off at higher temperatures due to trapped porosities. Compared to the densification curves, the lateral shrinkage of the micro-tubes followed a similar trend and achieved a maximum shrinkage of 25.8% at 1400 °C.

Fig. 2(a) and (b) present the photographs and SEM micrograph of the ScSZ micro-tubes fired at 1400 °C. The micro-tubes had approximately 3.8 mm in outer diameter, 39 mm in length, and 210 μm in thickness. No physical defects were visible on the fracture surfaces. Fig. 3 shows the SEM microstructures of the as-fired surfaces of the ScSZ micro-tubes fired respectively at 1100 °C, 1350 °C, 1400 °C, and 1450 °C. As revealed by Fig. 3(a), only neck growth and no densification were detected at the sintering temperature of 1100 °C. As the sintering temperature rose to 1350 °C and above, significant densification and grain growth were observed [Fig. 3(b)–(d)]. The average grain sizes of ScSZ sintered at 1350, 1400, and 1450 °C appeared to be 2.9 μm, 3.6 μm, and 4.4 μm respectively.

Fig. 4 shows the flexural strength and grain size of the micro-tubes as a function of sintering temperature. The flexural strength reported a lowest value of approximately 70 MPa at the sintering temperature of 1100 °C due to the high porosity content (31.7%). It was found that the flexural strength of the micro-tubes rose with increased sintering temperature due to the higher densification. Sintered at 1400 °C, the micro-tubes achieved a maximum flexural strength around 190 MPa, higher than those of the anode-supported tubular SOFCs reported in the literature [8,14]. As the sintering temperature escalated to 1450 °C, the flexural strength decreased slightly to approximately 171 MPa because of the coarser grain sizes of the ScSZ micro-tubes.

3.3. *Preparation and characteristics of the co-sintered electrolyte/anode bi-layers*

Table 3 summarizes the effects of the sintering conditions on the five anode-coated electrolyte micro-tubes prepared in this study. For sample Cell-01, the NiO/ScSZ anode layer was coated on the green ScSZ micro-tubes and then co-fired at 1300 °C. Results indicate that cracks existed near the anode surface while no evident crack was visible on the fracture surface of the anode layer. Also, the low co-sintering temperature led to poor mechanical strength which disqualifies the sample for practical applications. For sample Cell-02, the NiO/ScSZ anode layer coated on the green ScSZ micro-tube was co-sintered at 1400 °C. The microstructures of the cross-section fracture surface of the bi-layer and the sintered surface of the anode layer were shown in Fig. 5(a) and (b). Cracks were observed to extend through the whole anode layer and penetrate through the electrolyte layer, and trans-granular cracks were detected along nickel oxide grains. The resulting anode layer seemed too dense to create enough triple phase boundaries. For sample Cell-03, the NiO/ScSZ anode layer was dip-coated twice on the ScSZ micro-tubes pre-sintered at 1100 °C, and the anode layer had a similar thickness as those of samples Cell-01 and Cell-02. With the same anode slurry, the layer coated on the green ScSZ micro-tubes appeared to be almost twice thicker than those on the pre-sintered micro-tubes, suggesting that the porous and binder-containing surfaces of the green micro-tubes might exert a drag force on the anode slurry due to the capillary force

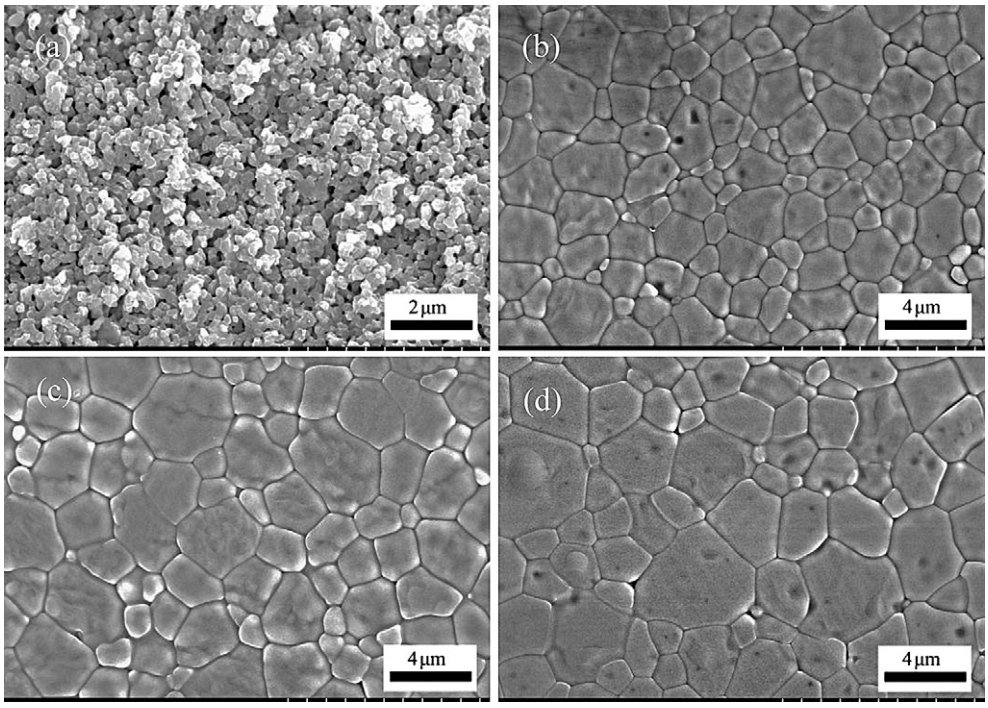

Fig. 3 – SEM micrographs of as-fired surfaces of ScSZ micro-tubes fired at (a) 1100 °C, (b) 1350 °C, (c) 1400 °C, and (d) 1450 °C.

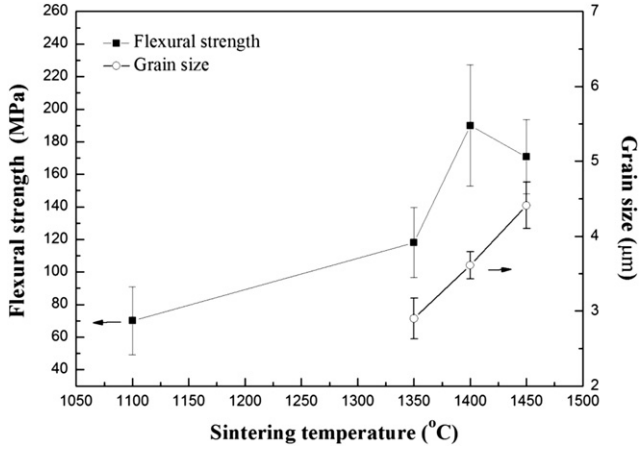

Fig. 4 – Flexural strength and average grain size of micro-tubes as a function of sintering temperature.

of the pores or the attractive force of the coupling binder agent. The electrolyte tube pre-sintered at 1100 °C reached a maximum theoretical density of 68%. The microstructures of the cross-section fracture surface of sample Cell-03 post-sintered at 1400 °C were presented in Fig. 5(e) and that of the sintered surface of the anode was shown in Fig. 5(f). No visible physical defect was detected on the porous anode layer with a thickness of ≈20 μm. For sample Cell-04, the anode layer was coated on the ScSZ micro-tube pre-sintered at 1200 °C and post-sintered at 1300 °C. After post-sintering, the anode layer fell off due to the shrinkage mismatch which weakened the interface bonding. For sample Cell-05, the NiO/ScSZ layer was coated on the ScSZ micro-tube pre- and post-sintered respectively at 1400 °C and 1250 °C. The microstructure of the cross-section fracture surface of sample Cell-05 after sintering was shown in Fig. 5(c) and that of the sintered surface of the anode in Fig. 5(d). A porous anode layer 6 μm in thickness was successfully prepared for attaching to the dense electrolyte micro-tube, which was pre-sintered at 1400 °C and reached a maximum theoretical density of ≈97%. Adhesion between the anode and electrolyte layer emerged to be superior to the one reported in the literature [15]. However, adhesion of the Ni-ScSZ anode layer on the electrolyte of sample Cell-05 was significantly degraded after reduction at 800 °C under 97% N_2–3%H_2 atmosphere, mainly because of the increase in porosity content associated with the reduction and the weakening of the cermet bonding due to the oxygen loss.

The mechanical integrity of the anode–electrolyte bi-layers is closely related to the coefficient of thermal expansion (CTE) during heating and cooling as well as the sintering shrinkage mismatch during co-sintering and the bonding strength at the interface of the bi-layers. In this study, it was observed that the coefficient of thermal expansion of the ScSZ ($\approx 12.3 \times 10^{-6}$ K^{-1}) was a little lower than that of the anode ($\approx 13.9 \times 10^{-6}$ K^{-1}) at temperatures ranging from room to 800 °C. It is expected that there was no significant thermal expansion mismatch among the components. As reported in the literature, the difference in the sintering shrinkage often leads to distortion of the planar-type multilayer ceramics, and controlling the powder characteristic, slurry formulation, and heating rate, and applying pressure during co-sintering are generally required to avoid warpage [16–20].

The dilatometric shrinkages of the green anode and the ScSZ compacts pre-sintered at 1100, 1200, 1400 °C were shown

Table 3 – Characteristics of sintered micro-tubes after different sintering conditions.

Sample no.	Sintering conditions		Thickness of anode layer (μm)	Characteristics of the sintered micro-tubes
	Pre-sintered temperature	Co-sintered temperature		
Cell-01	Green	1300 °C	~26	Slightly cracked
Cell-02	Green	1400 °C	~20	Cracked and ruptured
Cell-03	1100 °C	1400 °C	~20 (2 times)	Porous, excellent adhesion and strength
Cell-04	1200 °C	1300 °C	–	Delaminated
Cell-05	1400 °C	1250 °C	~6	Porous, poor adhesion and strength

in Fig. 6. The shrinkage profile with respect to the temperature of the ScSZ compacts was consistent with the sintered density with sintering temperature of the ScSZ micro-tube presented in Fig. 2. The ScSZ micro-tube started to densify at 860 °C and maximum shrinkage rate was observed at 1200 °C. A total of 22% shrinkage was observed as the temperature reached 1400 °C. After pre-sintering at 1100 °C, the ScSZ compact triggered no sintering shrinkage until 1040 °C. Sintering leveled off after 7.5% shrinkage at 1400 °C. Negligible shrinkages were observed for the ScSZ micro-tubes pre-sintered at 1200 and 1400 °C. For the anode compact consisting of NiO, ScSZ and carbon powders prepared from the anode slurry, small shrinkage was observed as the temperature escalated, and significant dimensional change was initiated at 700 °C. Totally, 30% shrinkage was obtained as the temperature reached 1400 °C.

Based on the sintering characteristics of electrolyte/anode micro-tubes listed in Table 3 and the dilatometrical shrinkage results of the electrolyte and anode materials shown in Fig. 6, the mechanical integrity of the electrolyte/anode micro-tubes after sintering can be clarified in term of sintering shrinkage mismatch. The anode layers of samples Cell-01 and Cell-02 shown in Table 3 densified during the co-sintering process associated with the green ScSZ micro-tubes while those of

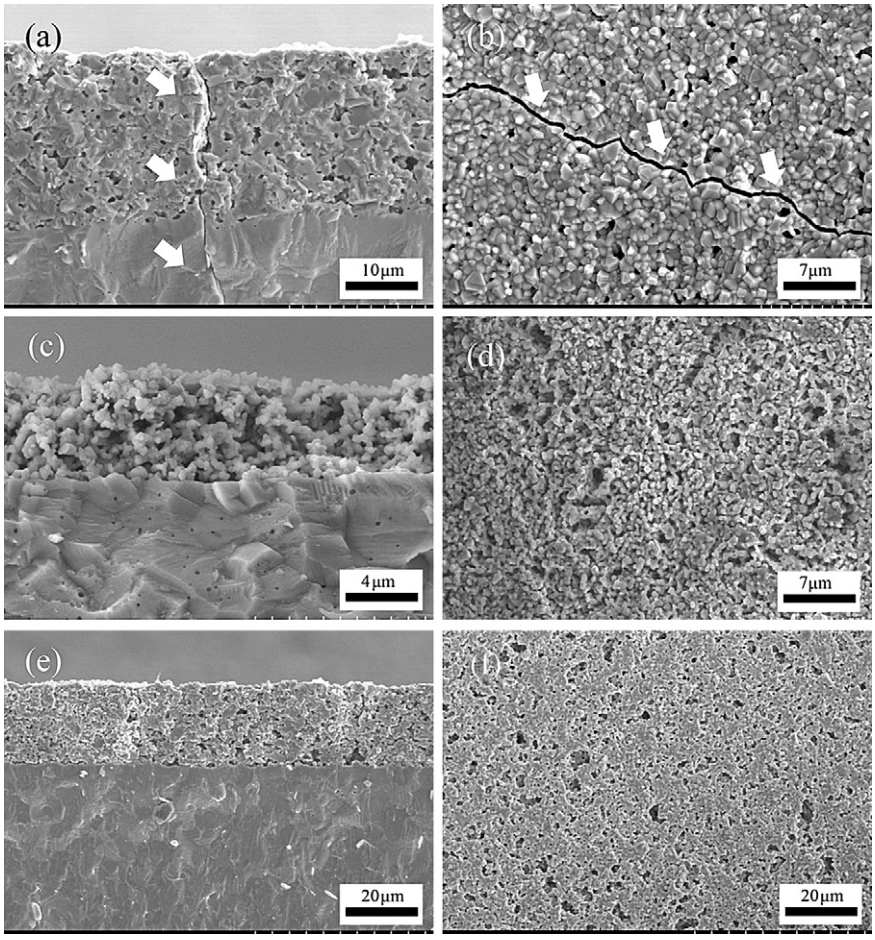

Fig. 5 – SEM micrographs of (a) cross-section of micro-tube and (b) as-fired anode surface of Cell-02; (c) cross-section of micro-tube and (d) as-fired anode surface of Cell-05; (e) cross-section of micro-tube and (f) as-fired anode surface of Cell-03.

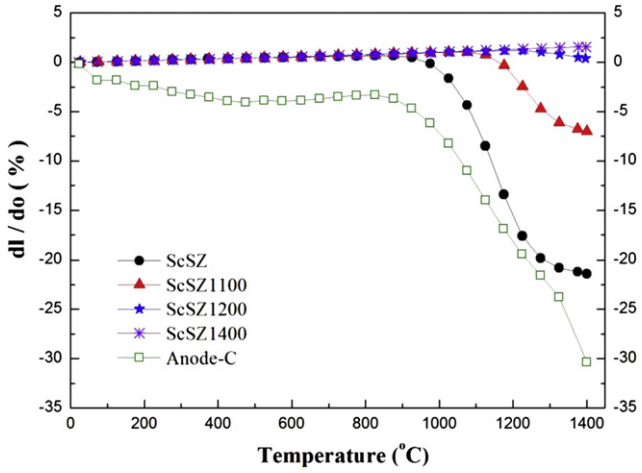

Fig. 6 – Shrinkage behavior of anode and ScSZ compact as a function of temperature.

samples Cell-03, Cell-04, and Cell-05 densified under constrained sintering on the pre-sintered ScSZ micro-tubes. In light of the above observations, densification of the anode layers was affected by different levels of stress depending on the sintering shrinkage mismatch which, together with the initial strength of the ScSZ micro-tubes, might impact the mechanical integrity of the final sintered micro-tubes. The difference in the sintering shrinkage during heating between layers triggered mismatch strain at the interface of the bi-layers during co-sintering or constrained sintering. The mismatch strains could be computed using the following formulas [21].

$$\text{Mismatch Strain} = \left(\frac{\Delta L}{L_0}\right)_{\text{ScSZ}} - \left(\frac{\Delta L}{L_0}\right)_{\text{Anode}} \quad (2)$$

Fig. 7(a) shows the mismatch strains of the anodes and electrolytes of samples Cell-01 and Cell-02 during co-sintering. For the green anode layers and green ScSZ micro-tubes at temperature up to 1300 or 1400 °C (Cell-01 and Cell-02 respectively), visible sintering mismatch strain (≈7.5%) was observed at temperatures below 1100 °C; as the temperature rose, the value fluctuated and finally reached ≈10% at 1400 °C. Smaller sintering shrinkage of the ScSZ micro-tube exerted a tension force on the thin anode layer, and cracks emerged on the anode surface at low temperatures. The stress concentrated around the crack tip and caused the cracks to expand into the electrolyte micro-tubes and finally led to the rupture of the bi-layers as the shrinkage mismatch magnified with the rising temperature. Fig. 7(b) reveals the mismatch strains of the anode layers on the ScSZ micro-tubes pre-sintered at 1100, 1200, and 1400 °C (Cell-03, Cell-04, and Cell-05 respectively) during constrained sintering. The thick pre-fired ScSZ micro-tubes were strong enough to retain their mechanical integrity when subjected to the stress caused by the sintering mismatch. However, the pre-sintered ScSZ micro-tubes were likely to place a tension force on the green anode layer during densification. Cracks and delamination would be initiated if the shrinkage mismatch reached a certain level, particularly

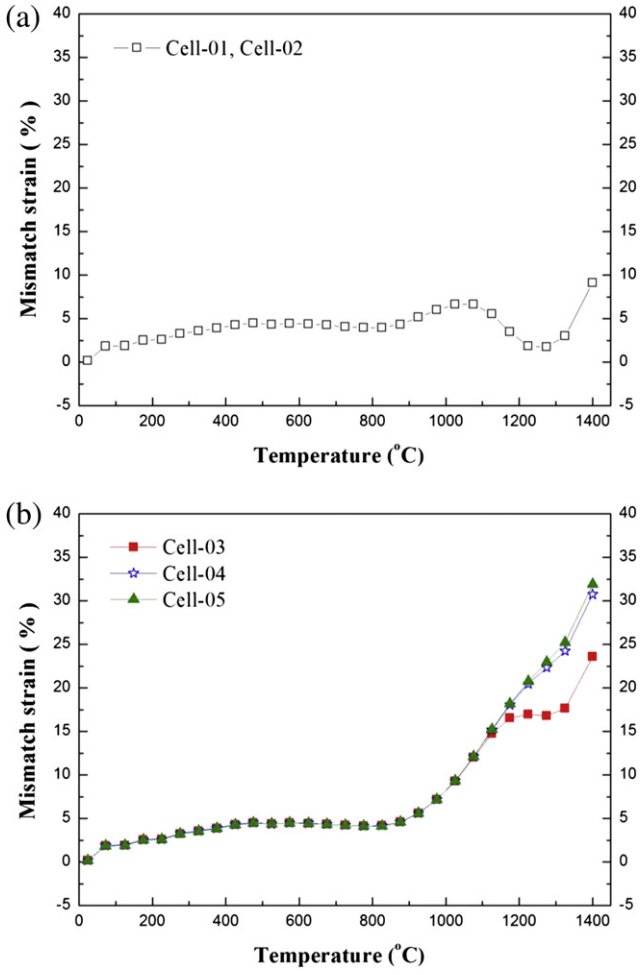

Fig. 7 – Mismatch strains of (a) anode and electrolyte of Cell-01 and Cell-02 samples during co-sintering, and (b) anode and pre-sintered electrolyte of Cell-03, Cell-04, and Cell-05 samples during constrained sintering.

during the final-stage sintering of the anode layer. For samples Cell-04 and Cell-05, the ScSZ micro-tubes were well densified before sintering with the anode layer and revealed almost no shrinkage at temperatures up to 1400 °C. Significant mismatch strain up to ≈32.5% was accumulated and activated a huge tension force on the thin anode layer, inhibiting anode densification and resulting in highly porous anode layers as shown in Fig. 5(c) and (d). However, similar to the cases of sample Cell-04 and Cell-05, the ScSZ micro-tube of sample Cell-03 pre-sintered at 1100 °C revealed no shrinkage below 1150 °C. The tube, however, experienced a sintering shrinkage of ≈7.5% at temperatures ranging from 1150 to 1400 °C; the shrinkage mismatch strain was minimized to a range from 32.5% to 23.5% during the final-stage sintering of the anode layer, thereby enabling the bi-layer to maintain better mechanical integrity and the anode layer to achieve better densification [Fig. 5(e) and (f)]. It appeared that the porosity of the anode could be precisely monitored by the level of the sintering shrinkage of the ScSZ tubular substrate during constrained sintering, which is similar to those observed in the literature [6,7,22–24].

3.4. *Preparation and characterization of SOFC single cell*

To prepare the SOFC single cell, a LSM layer was coated on the outer surface of sample Cell-03 via dip-coating and then post-sintered at 1200 °C, after a thin NiO layer was coated on the top of the composite anode and fired at 1350 °C to enhance the current collection of the anode. After thermal cycling between 30 °C and 800 °C under 97% N_2–3%H_2 on the anode site and air on the cathode site for 10 times at a heating rate and a cooling rate of 5 °C/min, the micro-tubular SOFC retained a good mechanical integrity as indicated by the SEM results presented in Fig. 8. With its thickness controlled at ≈34 μm, the LSM cathode layer demonstrated a good interconnecting porosity and a fine grain microstructure. No crack or delamination in the multilayer structure was visible. The formulation and processing for fabricating tubular SOFC single cells were successfully developed. Fig. 9 shows the *I*–*V* curves and the corresponding power densities of the micro tubular SOFC, containing a ScSZ electrolyte, a LSM–GDC composite cathode, and an anode composed of a NiO–ScSZ composite layer and a NiO layer, measured at different temperatures. At 920 and 900 °C, the maximum power densities (MPD) of the single cell read respectively 0.26 and 0.23 W cm^{-2} and the open circuit voltage (OCV) reported the same 1.08 V. These MPD values are comparable to that (0.17 W cm^{-2}) of a planar type SOFC with a similar structure and fabrication process prepared in this study. Further enhancement on the cell performance is expected by optimizing the electrode materials and their microstructures.

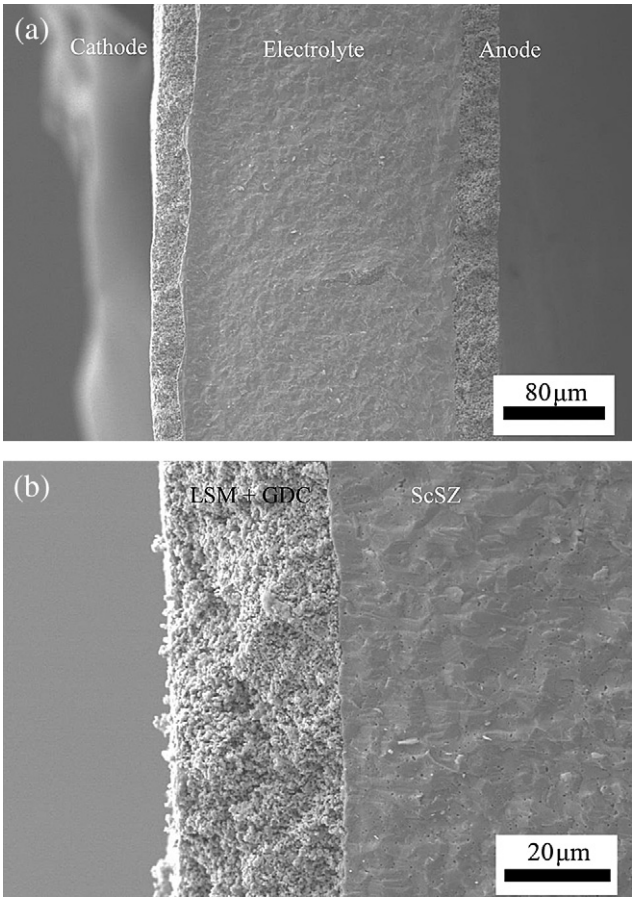

Fig. 8 – SEM micrographs of (a) micro tubular SOFC and (b) cathode layer.

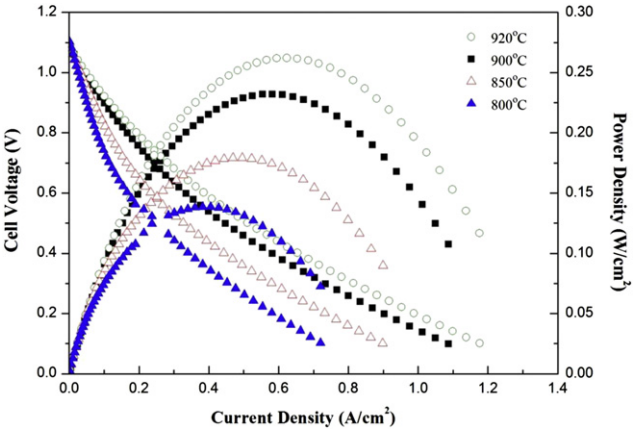

Fig. 9 – *I*–*V* curves and the corresponding power densities of the micro tubular SOFC, containing a ScSZ electrolyte, a LSM–GDC composite cathode, and an anode composed of a NiO–ScSZ composite layer and a NiO layer, measured at different temperatures.

4. Conclusion

In this study, electrolyte-supported tubular SOFCs were fabricated using extrusion and dip-coating. The characteristics of the micro-tubes extruded were found to depend on paste formulation. The ScSZ-21b paste emerged as the best formulation to produce the dense electrolyte micro-tubes with a theoretical density of 97.1% and a bending strength of 190 MPa after sintering at 1400 °C. Densification behavior of the anode on the tubular electrolyte support appeared to take place during either the co-sintering process or the constrained sintering processing. The anode layer of ScSZ–NiO coated on the ScSZ micro-tube pre-sintered at 1100 °C and post-sintered at 1400 °C was observed to achieve a better mechanical integrity. LSM–GDC cathode layer was then coated on the outer surface of the micro-tubes and post-sintered at 1100 °C. The MPD of the tubular Ni–ScSZ/ScSZ/GDC–LSM cell with an electrolyte thickness of 210 μm read 0.26 and 0.23 W cm^{-2} respectively at 920 and 900 °C, and OCV reported the same 1.08 V.

REFERENCES

[1] Badwal SPS, Foger K. Solid oxide electrolyte fuel cell review. Ceramics International 1996;22:257–65.
[2] Yamamoto O. Solid oxide fuel cells fundamental aspects and prospects. Electrochimca Acta 2000;45:2423.
[3] Howe KS, Thompson GJ, Kendall K. Micro-tubular solid oxide fuel cells and stacks. Journal of Power Sources 2011;196:1677–86.

[4] Suzuki T, Funahashi Y, Yamaguchi T, Fujishiro Y, Awano Masanobu. Design and fabrication of lightweight, submillimeter tubular solid oxide fuel cells. Electrochemical and Solid-State Letters 2007;10(8):177–9.
[5] Kanawka K, Dal Grande F, Wu Z, Thursfield A, Ivey D, Metcalfe I, et al. Microstructure and performance investigation of solid oxide fuel cells bases on highly asymmetric YSZ microtubular electrolytes. Industrial & Engineering Chemistry Research 2010;49:6062–8.
[6] Yamaguchi T, Suzuki T, Shimizu S, Fujishiro Y, Awano M. Examination of wet coating and co-sintering technologies for micro-SOFCs fabrication. Journal of Membrane Science 2007; 300:45–50.
[7] Morales M, Navarro ME, Capdevila XG, Roa JJ, Segarra M. Processing of graded anode-supported micro-tubular SOFCs based on samaria-doped ceria via gel-casting and spray-coating. Ceramics International 2012;38:3713–22.
[8] Zhang X, Lin B, Ling Y, Dong Y, Meng G, Liu X. An anode-supported micro-tubular solid oxide fuel cell with redox stable composite cathode. International Journal of Hydrogen Energy 2010;35:8654–62.
[9] Dollard WJ. Journal of Power Sources 1992;37(1–2):133–9.
[10] Kendall K, Palin M. A small solid oxide fuel cell demonstrator for microelectronic applications. Journal of Power Sources 1998;71:268–70.
[11] Herlea JV, Ihringer R, Sammes NM, Tompsett G, Kendall K, Yamada K, et al. Concept and technology of SOFC for electric vehicles. Solid State Ionics 2000;132:333–42.
[12] Faes A, Nakajo A, Hessler-Wyser A, Dubois D, Brisse A, Modena S, et al. RedOx study of anode-supported solid oxide fuel cell. Journal of Power Sources 2009;193:55–64.
[13] Händle Frank. Extrusion in ceramics. New York: Springer Berlin Heidelberg; 2010. pp. 327.
[14] Sammes NM. The mechanical properties of tubular solid oxide fuel cells. Journal of Materials Science 2003;38:4811–6.
[15] Mallon C, Kendall K. Sensitivity of nickel cermet anodes to reduction conditions. Journal of Power Sources 2005;145: 154–60.
[16] Shen Z, Zhu X, Le S, Sun W, Sun K. Co-sintering anode and Y_2O_3 stabilized ZrO_2 thin electrolyte film for solid oxide fuel cell fabricated by co-tape casting. International Journal of Hydrogen Energy 2012;37:10337–45.
[17] Bao W, Chang Q, Meng G. Effect of NiO/YSZ compositions on the co-sintering process of anode-supported fuel cell. Journal of Membrane Science 2005;259:103–9.
[18] Park HG, Moon H, Park SC, Lee JJ, Yoon D, Hyuna SH, et al. Performance improvement of anode-supported electrolytes for planar solid oxide fuel cells via a tape-casting/ lamination/co-firing technique. Journal of Power Sources 2010;195:2463–9.
[19] Lee SH, Messing GL, Awano M. Sintering arches for cosintering camber-free SOFC multilayers. Journal of the American Ceramic Society 2008;91(2):421–7.
[20] Le S, Sun KN, Zhang N, Zhu X, Sun H, Yuan YX, et al. Fabrication and evaluation of anode and thin Y_2O_3-stabilized ZrO_2 film by co-tape casting and co-firing technique. Journal of Power Sources 2010;195:2644–8.
[21] Bordia RK, Olevsky EA. Advances in sintering science and technology. Ceramic Transactions 2009;209:311.
[22] Fu1 C, Ge X, Chan SH, Liu Q. Fabrication and characterization of anode-supported low-temperature SOFC based on Gd-doped ceria electrolyte. Fuel Cells 2012;3:450–6.
[23] Wei CC, Li K. Yttria-stabilized zirconia (YSZ)-based hollow fiber solid oxide fuel cells. Industrial & Engineering Chemistry Research 2008;47:1506–12.
[24] Kanawka K, Grande FD, Wu Z, Thursfield A, Ivey D, Metcalfe I, et al. Microstructure and performance investigation of a solid oxide fuel cells based on highly asymmetric YSZ microtubular electrolytes. Industrial & Engineering Chemistry Research 2010;49:6062–8.